Front. Phys. 11(3), 115201 (2016)
DOI 10.1007/s11467-015-0545-2

RESEARCH ARTICLE

Potential distribution around a test charge in a positive dust-electron plasma

S. Ali

National Centre for Physics (NCP) at Quaid-e-Azam University Campus, Shahdra Valley Road, Islamabad 44000, Pakistan

E-mail: shahid.ali@ncp.edu.pk

Received July 26, 2015; accepted October 17, 2015

The electrostatic potential caused by a test-charge particle in a positive dust-electron plasma is studied, accounting for the dust-charge fluctuations associated with ultraviolet photoelectron and thermionic emissions. For this purpose, the set of Vlasov–Poisson equations coupled with the dust charging equation is solved by using the space–time Fourier transform technique. As a consequence, a modified dielectric response function is obtained for dust-acoustic waves in a positive dust-electron plasma. By imposing certain conditions on the velocity of the test charge, the electrostatic potential is decomposed into the Debye–Hückel (DH), wake-field (WF), and far-field (FF) potentials that are significantly modified in the limit of a large dust-charge relaxation rate both analytically and numerically. The results can be helpful for understanding dust crystallization/coagulation in two-component plasmas, where positively charged dust grains are present.

Keywords dusty plasmas, dust charge fluctuations, positively charged dusty plasma, shielding and dynamical potentials

PACS numbers 52.25.Dg, 52.27.Lw

1 Introduction

For several decades, the topics of energy loss and the potential distributions around a test charge have remained the focus of researchers owing to the potential implications in both electron-ion plasmas [1–5] and multicomponent dusty plasmas [6–11]. A static or slowly moving test charge polarizes the plasma medium, and as a result, a cloud of charges with opposite signs shields the test-charge particle, giving rise to a short-range Debye–Hückel (DH) potential or long-range far-field (FF) potential. However, a test charge that resonantly interacts with a plasma wave forms an oscillatory wake field (WF) behind it. This WF consists of a negative (positive) potential region, which may lead to the creation of regular crystalline structures [6, 7] by trapping positive (negative) ions. As a consequence, attractive forces appear among the negatively (positively) charged dust grains with the same polarity in dusty plasmas. Hence, the WF potential can play a significant role in the formation of organized (ordered) structures of dust grains known as dusty crystals [12]. The crystallization of dust grains has been confirmed in many laboratory experiments in the past [13–17]. First, Nambu and Akama [18] introduced the concept of an attractive WF potential due to the collective interaction of a test charge with an ion-acoustic wave in an electron-ion plasma.

However, the inclusion of a dust component makes the conventional electron-ion plasma more complex, and one of the reasons for this complexity is the dust-charge fluctuations on the dust-grain surface. Dust grains can be either positively or negatively charged, mainly depending upon the ambient plasma and dust-grain surface potential. The charge on the dust particulates (grains) does not always remain constant, but it fluctuates about the equilibrium charge state owing to the fluctuating electric field. Numerous investigations [19–23] have been carried out to investigate the effects of dust-charge fluctuations on the spectrum of dust-acoustic (DA) and dust-ion-acoustic (DIA) waves by simply considering the dust grains as negatively charged particles. Nasim and his coauthors [24, 25] employed the theory of dust-charge perturbation caused by the collection of electron and ion currents onto the dust-grain surface and presented analytical and numerical calculations for a test-charge potential and the energy loss in a negatively charged dusty plasma. Later on, Ali *et al.* [26] decomposed the shielded potential into the DH and WF potentials, accounting for the small and large dust-charge relaxation rates of

negatively charged dust grains. Noticeable modifications in the shapes of the DH and WF potentials appeared in the case of single and multiple test charges owing to the variation in different plasma parameters such as the speed of the test charge, the dust-neutral collision, and dust-charging and/or relaxation rates.

There are many space [27, 28] and laboratory [29, 30] environments in which positively charged dust grains are present. The generation of positive charge on the dust grains could be caused by other charging mechanisms, namely, ultraviolet photoelectron emission [31], thermionic emission [29], secondary electron emission [32], etc. In this context, Shukla [33] employed the fluid equations to re-examine the dispersive properties of DA waves in an unmagnetized thermal dusty (dust-electron) plasma [34]. It was shown that the electron collection, thermionic, and photoelectron emission currents significantly modify the frequency of the DA wave and the damping rate. Later, the work was extended [32] to incorporate the dust-charge perturbations by the orbital motion limited (OML) and secondary electron currents in an unmagnetized dusty plasma containing both positively and negatively charged dust grains [28, 35, 36]. In particular, Delzanno *et al.* [37] presented simulation work involving the thermionic electron emission current to study the attractive dynamical potential and highlighted the possibility of ordered structures of positively charged dust particles [30]. Recently, Paul [38] investigated the linear properties of DA waves in a dusty plasma to account for the charge-fluctuating inertial positive dust and charge-fluctuating static negative dust both analytically and numerically.

In this paper, we calculate the potential distribution around a test charge moving with a constant speed along the z axis in a positive dust-electron plasma, whose constituents are the inertialess electrons and positively charged mobile dust grains. The set of Vlasov–Poisson equations coupled with the dust charging equation is solved to derive expressions for the DH, WF, and FF potentials in the limit of a large dust-charge relaxation rate. One of the main objectives is to examine the impact of dust-charge fluctuations caused by thermionic and ultraviolet photoelectron emission on the profiles of the shielded potential in a positive dust-electron plasma.

This manuscript is organized as follows. In Section 2, linearized kinetic theory is employed for the derivation of the modified dielectric function involving DA waves and the test-charge potential caused by dust-charge variations in a positive dust-electron plasma. In Section 3, the electrostatic potential is decomposed into the DH and WF potentials, and the large dust-charge relaxation rate is taken into account. Section 4 presents the shielded potential in terms of the FF potential, exhibiting a decay that depends on the inverse cube of both the axial and radial distances from the test charge in a positive dust-electron plasma. Numerical results are discussed and summarized in Section 5.

2 Test-charge potential in a positive dust-electron plasma

An unmagnetized collisionless dusty plasma is considered, which consists of electrons and positively charged massive dust particulates (grains). For low-phase-velocity DA perturbations, the inertia mainly comes from the positively charged dust particulates having a constant mass m_d and radius R, whereas the electrons play their role through the Boltzmann distribution, i.e., $n_{e1} \approx n_{e0}e\phi_1/T_e$, where n_{e1} (n_{e0}) is the perturbed (equilibrium) electron number density, T_e is the electron temperature in energy units, and e is the magnitude of the electronic charge. At equilibrium, the charge-neutrality condition $n_{e0} = Z_{d0}n_{d0}$ holds. The equilibrium dust-charge state and equilibrium number density for positively charged dust grains are denoted by Z_{d0} and n_{d0}, respectively. The dynamics of the DA waves in a positively charged (viz., $Z_{d0}e > 0$) unmagnetized dusty plasma can be governed by the following linearized Vlasov–Poisson set of equations:

$$\left(\frac{\partial}{\partial t} + \boldsymbol{V}\cdot\nabla\right) f_{d1} + \frac{Z_{d0}e}{m_d}\boldsymbol{E}_1\cdot\nabla_{\boldsymbol{v}}\ f_{d0} = 0, \tag{1}$$

and

$$\nabla^2\phi_1 = -4\pi e\left(-n_{e1} + Z_{d1}n_{d0} + Z_{d0}\int f_{d1}\mathrm{d}\boldsymbol{V}\right) - 4\pi Q_t\delta\left(\boldsymbol{r} - \boldsymbol{V}_t t\right), \tag{2}$$

where $f_{d1}(\ll f_{d0})$ represents the perturbed (equilibrium) dust particle distribution function, and $\boldsymbol{E}_1(=-\nabla\phi_1)$ is the induced electric field involving ϕ_1 as an induced electrostatic potential. The last term on the R.H.S of Eq. (2) is the test-charge density of a test charge Q_t, which propagates in a positive dust-electron plasma with a constant velocity $\boldsymbol{V}_t$ along the z axis. The symbol $\delta\left(\boldsymbol{r} - \boldsymbol{V}_t t\right)$ stands for a three dimensional Dirac delta function, where the position vector $\boldsymbol{r}$ represents an observation point. The effect of the dust-charge variation enters through the perturbed charging state Z_{d1}, indicating that the charge on the dust is not fixed but fluctuates in space and time owing to the fluctuating electric field and significantly depends on the ambient plasma and dust-grain surface potential. The dust may be negatively charged owing to the fluctuating currents of electrons and

ions on the dust-grain surface, which strongly affects the collective modes and instabilities in dusty plasmas [39]. In particular, charging mechanisms such as thermionic and ultraviolet photoelectron emissions lead to a positive charge ($eZ_d > 0$) on the dust particulates. Thus, the dust charging equation for positively charged particulates can be defined as

$$\partial_t Z_d e = I_e + I_{th} + I_{ph}, \tag{3}$$

where I_e is the electron collection current on the dust-grain surface, and I_{th} and I_{ph} are the thermionic and photoelectron emission currents, respectively. These currents [40–42] can be written in the following form under the assumption $T_d = T_e$:

$$I_e = -\frac{4\pi R^2}{\sqrt{2\pi}} e n_e V_{te} \left(1 + \chi_e\right),$$

$$I_{th} = 4\pi R^2 e \left(\frac{m_e T_e}{2\pi\hbar^2}\right)^{3/2} \sqrt{\frac{2}{\pi}} V_{te} \left(1 + \chi_e\right) \times \exp\left(\frac{-W_e}{T_e} - \chi_e\right),$$

and

$$I_{ph} = \pi e R^2 J Y \exp(-\sigma\chi_e),$$

where $V_{te}[= \left(T_e/m_e\right)^{1/2}]$ is the thermal speed of an electron, $\sigma\,(= T_e/T_{ph})$ is the ratio of the electron-to-photoelectron thermal energies, $\chi_e\,(= e\varphi/T_e)$ corresponds to the potential energy-to-thermal-energy ratio, and $\varphi(= eZ_d/R)$ represents the dust-grain surface potential. The ultraviolet photon flux and the yield of the photons are denoted by J and Y, respectively. Further, W_e stands for the electron work function, $\omega_{pe} = \left(4\pi n_{e0} e^2/m_e\right)^{1/2}$ is the electron plasma frequency, m_e is the electron mass, and $\hbar$ is the Planck constant divided by 2π.

By expressing Eq. (3) in terms of equilibrium and perturbed quantities, i.e., $\chi_e = \chi_{e0} + \chi_{e1}$, $n_e = n_{e0} + n_{e1}$, and $Z_d = Z_{d0} + Z_{d1}$, a linearized dust-charging equation is obtained as

$$\partial_t Z_{d1} e = I_{e1} + I_{th1} + I_{ph1} \tag{4}$$

with the perturbed currents

$$I_{e1} = -\frac{4\pi R^2}{\sqrt{2\pi}} e n_{e0} V_{te} \left[\frac{e^2 Z_{d1}}{R T_e} + \left(1 + \chi_{e0}\right)\frac{e\phi_1}{T_e}\right],$$

$$I_{th1} = -eZ_{d1}\frac{R\omega_{pe}}{\lambda_{De}}\sqrt{\frac{2}{\pi}}\frac{\chi_{e0}}{n_{e0}}\left(\frac{m_e T_e}{2\pi\hbar^2}\right)^{3/2} \times \exp\left(-\frac{W_e}{T_e} - \chi_{e0}\right),$$

and

$$I_{ph1} = -\frac{eZ_{d1} R\omega_{pe}}{4\lambda_{De}}\frac{\sigma J Y}{n_{e0} V_{te}} \exp\left(-\sigma\chi_{e0}\right),$$

where $\lambda_{De}\ [= \left(T_e/4\pi e^2 n_{e0}\right)^{1/2}]$ represents the electron Debye length. Equation (4) can be expressed in a more simplified form as

$$\left(\partial_t + \nu_r\right) eZ_{d1} = -R\nu_a\phi_1. \tag{5}$$

The dust-charge relaxation and electron absorption rates can be respectively defined as

$$\nu_r = \frac{R}{\sqrt{2\pi}}\frac{\omega_{pe}^2}{V_{te}}\left[1 + 2\left(\frac{m_e T_e}{2\pi\hbar^2}\right)^{3/2}\frac{\chi_{e0}}{n_{e0}} \times \exp\left(\frac{-W_e}{T_e} - \chi_{e0}\right) + \frac{\sqrt{2\pi}\sigma J Y}{4n_{e0} V_{te}}\exp\left(-\sigma\chi_{e0}\right)\right] \tag{6}$$

and

$$\nu_a = \frac{R}{\sqrt{2\pi}}\frac{\omega_{pe}^2}{V_{te}}\left(1 + \chi_{e0}\right). \tag{7}$$

Note that the dust-relaxation rate involves the contribution of both the thermionic and photoelectron emission currents in addition to the electron collection current. Moreover, the absorption rate only includes the electron collection current. By applying of the space–time Fourier transform technique to Eqs. (1), (2), and (5), we obtain the following expressions:

$$\tilde{f}_{d1}(\boldsymbol{k},\omega) = -\frac{eZ_{d0}}{m_d}\frac{\boldsymbol{k}\cdot\nabla_{\boldsymbol{v}} f_{d0}\tilde{\phi}_1\left(\boldsymbol{k},\omega\right)}{\left(\omega - \boldsymbol{k}\cdot\boldsymbol{V}\right)}, \tag{8}$$

$$k^2\tilde{\phi}_1\left(\boldsymbol{k},\omega\right) = 4\pi e\left[-\tilde{n}_{e1}\left(\boldsymbol{k},\omega\right) + Z_{d0}\int \tilde{f}_{d1}\left(\boldsymbol{k},\omega\right)\mathrm{d}\boldsymbol{V} + n_{d0}\tilde{Z}_{d1}\left(\boldsymbol{k},\omega\right)\right] + 4\pi Q_t\int \exp\left(-\mathrm{i}\left(\boldsymbol{k}\cdot\boldsymbol{V}_t - \omega\right)t\right)\mathrm{d}t, \tag{9}$$

and

$$4\pi e\tilde{Z}_{d1}\left(\boldsymbol{k},\omega\right)n_{d0} = -\frac{\beta\tilde{\phi}_1\left(\boldsymbol{k},\omega\right)}{\lambda_{De}^2\left(\mathrm{i}\omega + \nu_r\right)}, \tag{10}$$

where ω (k) is the wave frequency (wave number), $\tilde{n}_{e1}\left(\boldsymbol{k},\omega\right)\left(\approx n_{e0}e\tilde{\phi}_1/T_e\right)$ is the Fourier-transformed perturbed electron number density, $\tilde{Z}_{d1}$ is the Fourier-transformed perturbed dust charging state, and $\beta = 4\pi n_{d0}\nu_a R\lambda_{De}^2$. By simplifying Eqs. (8)–(10) together, the electrostatic potential in ω–$\boldsymbol{k}$ space becomes

$$\tilde{\phi}_1\left(\boldsymbol{k},\omega\right) = \frac{8\pi^2 Q_t\delta\left(\omega - \boldsymbol{k}\cdot\boldsymbol{V}_t\right)}{k^2 D\left(k,\omega\right)}. \tag{11}$$

The important point is to note that the dust charge fluctuation significantly modifies the dielectric constant $D\left(k,\omega\right)$ of the DA waves, which can be written as

$$D(k,\omega)=1+\frac{1}{k^2\lambda_{De}^2}+\frac{W(C_d)}{k^2\lambda_{Dd}^2}+\frac{1}{k^2\lambda_{De}^2}\frac{\beta}{\nu_r+\mathrm{i}\omega}, \quad (12)$$

where $W(C_d)\left[=(\pi)^{-1/2}\int_{-\infty}^{\infty}q\exp\left(-q^2\right)/(q-C_d)\,\mathrm{d}q\right]$ represents the well-known plasma dispersion function [43] for dust species with a dust thermal speed $V_{td}[=(T_d/m_d)^{1/2}]$ and a dust Debye length $\lambda_{Dd}=\left(T_d/4\pi e^2Z_{d0}^2n_{d0}\right)^{1/2}$. By assuming $C_d\,(=\omega/kV_{td})>1$ and $\omega<\nu_r$, Eq. (12) can be simplified to the following form:

$$D(k,\omega)=1+\frac{1}{k^2\lambda_{De}^2}-\frac{\omega_{pd}^2}{\omega^2}+\frac{1}{k^2\lambda_{De}^2}\frac{\beta}{\nu_r}. \quad (13)$$

For $D(k,\omega)=0$, a dispersion relation for DA waves is obtained, accounting for the large dust-charge relaxation rate in a positively charged dusty plasma. Equation (13) exactly coincides with the previous result [33] under the assumptions $kV_{td}\ll\omega$ and $\omega\gg\nu_d$, where ν_d is the dust-neutral collision frequency. After taking the inverse Fourier transformation of Eq. (11) and integrating with respect to ω, we obtain [44]

$$\phi_1(\boldsymbol{r},t)=\frac{Q_t}{2\pi^2}\int\frac{\exp\left[\mathrm{i}\boldsymbol{k}\cdot(\boldsymbol{r}-\boldsymbol{V}_t t)\right]}{k^2D(k,\boldsymbol{k}\cdot\boldsymbol{V}_t)}\mathrm{d}\boldsymbol{k}. \quad (14)$$

This is the electrostatic potential caused by a test charge moving at a constant velocity $\boldsymbol{V}_t$ along the z axis in a positively charged fluctuating dusty plasma. It is important to mention here that DA waves in a thermal dusty plasma have already been studied [33] by incorporating the dust-charge fluctuations due to thermionic emission and ultraviolet photoemission. In the framework of fluid theory [45, 46], it was analytically shown that dust charging effects modify not only the spectrum of the DA waves but also the spatiotemporal damping rates. Conversely, we utilize the Vlasov–Poisson model to calculate the potential distributions around a test charge by using the dielectric constant of the DA waves in an electron-dust thermal plasma. Different conditions are imposed on the speed of the test charge in comparison with the thermal speeds of the plasma species to derive the expressions for the Debye, WF, and FF potentials in the limit of a large dust-charge relaxation rate. Numerically, the results are analyzed for typical laboratory parameters to reveal the new impacts of dust-charge fluctuations on the profiles of the potentials.

Thus, the electrostatic potential in Eq. (14) is solved in either spherical polar or cylindrical coordinates for two specific cases: (i) $V_t\simeq\omega/k$ and (ii) $V_t\ll V_{td}$. In fact, the choice of a coordinate system depends upon the motion and speed of the test charge; a test charge at rest or slowly moving leads to a spherically symmetric potential distribution around it. However, as the test charge moves at a finite speed in a specific direction, the potential distribution (WF) appears behind the test charge and can be appropriately solved in the cylindrical coordinate system.

3 DH and WF potentials with a large dust-charge relaxation rate

In the limit of a large relaxation rate, i.e., $\nu_r>\boldsymbol{k}\cdot\boldsymbol{V}_t$, the inverse of the dielectric constant in Eq. (13) can be written as

$$D^{-1}=\frac{k^2\lambda_{De}^2/\left(1+\frac{\beta}{\nu_r}\right)}{k^2\lambda_{De}^2/\left(1+\frac{\beta}{\nu_r}\right)+1}\left[1+G(\boldsymbol{k}\cdot\boldsymbol{V}_t)\right], \quad (15)$$

where the dynamical function is given by

$$G(\boldsymbol{k}\cdot\boldsymbol{V}_t)=\frac{\omega_k^2}{(\boldsymbol{k}\cdot\boldsymbol{V}_t)^2-\omega_k^2}. \quad (16)$$

The square of the DA wave frequency is given by

$$\omega_k^2=\frac{\omega_{pd}^2k^2\lambda_{De}^2/\left(1+\frac{\beta}{\nu_r}\right)}{k^2\lambda_{De}^2/\left(1+\frac{\beta}{\nu_r}\right)+1}. \quad (17)$$

By substituting Eq. (15) into Eq. (14), we can respectively decompose the electrostatic potential into the DH and WF potentials as

$$\phi_{DH}=\frac{Q_t}{2\pi^2}\int\mathrm{d}\boldsymbol{k}\frac{\lambda_{De}^2/\left(1+\frac{\beta}{\nu_r}\right)}{k^2\lambda_{De}^2/\left(1+\frac{\beta}{\nu_r}\right)+1}\times\exp\left[\mathrm{i}\boldsymbol{k}\cdot(\boldsymbol{r}-\boldsymbol{V}_t t)\right] \quad (18)$$

and

$$\phi_{WF}=\frac{Q_t}{2\pi^2}\int\mathrm{d}\boldsymbol{k}\frac{G(\boldsymbol{k}\cdot\boldsymbol{V}_t)\lambda_{De}^2/\left(1+\frac{\beta}{\nu_r}\right)}{k^2\lambda_{De}^2/\left(1+\frac{\beta}{\nu_r}\right)+1}\times\exp\left[\mathrm{i}\boldsymbol{k}\cdot(\boldsymbol{r}-\boldsymbol{V}_t t)\right]. \quad (19)$$

Equation (18) can be solved by using spherical polar coordinates to obtain the DH potential as

$$\phi_{DH}(\boldsymbol{r},t)=\frac{Q_t}{r}\exp\left(\frac{-r}{\lambda_{De}/\left(1+\frac{\beta}{\nu_r}\right)^{1/2}}\right), \quad (20)$$

where $r=\left(\rho^2+\xi^2\right)^{1/2}$ is the distance of the test charge from an observation point $\boldsymbol{r}$ with its radial and axial distances $\rho\,(=r\sin\theta_r)$ and $\xi\,(=z-V_t t)$. It may be noted that the DH potential in Eq. (20) is significantly modified owing to the large dust-charge relaxation rate (viz.,

$\boldsymbol{k}\cdot\boldsymbol{V}_t < \nu_r$) due to the effects of the ultraviolet photoelectron and thermionic emission current. To proceed further, we simplify the WF potential in Eq. (19) in cylindrical coordinates by using standard techniques [6–10] as

$$\phi_{WF}(\rho=0,\xi) \approx \frac{2Q_t}{\xi}\left[1+\frac{C_{da}^2}{V_t^2\left(1+\frac{\beta}{\nu_r}\right)}\right] \times \left[1-\frac{C_{da}^2}{V_t^2\left(1+\frac{\beta}{\nu_r}\right)}\right]^{-1}\cos\left(\frac{\omega_{pd}\xi}{V_t}\right). \quad (21)$$

This is the WF potential of a test charge moving with a constant velocity V_t along the z axis in a positive dust-electron plasma, accounting for a large dust-charge relaxation rate. Note that the WF potential becomes an attractive potential [6-10] under the conditions $V_t(1+\beta/\nu_r) > C_{da}(\equiv \omega_{pd}\lambda_{De})$ and $\cos(\omega_{pd}\xi/V_t) < 0$. Hence, the attractive WF potential could be responsible for attracting the positive dust grains of the same polarity so that crystalline structures can be formed in a positively charged dusty plasma [30].

4 DH and FF potentials with a large dust-charge relaxation rate

In this case, we consider a test charge Q_t moving at a constant speed V_t along the z axis in a positively charged fluctuating dusty plasma and calculate the potential distribution around it. For this, the condition $V_t \ll V_{td}$ is imposed on the speed of the test charge, which indicates that the test charge is moving much slower than the massive dust species, and consequently, the test charge does not resonate with the phase speed of the DA waves. Therefore, no WF appears behind the test charge. In the limit of a large dust-charge relaxation rate ($\boldsymbol{k}\cdot\boldsymbol{V}_t < \nu_r$), Eq. (12) can be expressed for a slow test-charge response as

$$D(k,\boldsymbol{k}\cdot\boldsymbol{V}_t) = 1+\frac{1}{k^2\lambda_{De}^2}+\frac{1}{k^2\lambda_{Dd}^2} \times\left[1+\mathrm{i}\sqrt{\frac{\pi}{2}}C_d\exp\left(\frac{C_d^2}{2}\right)\right]+\frac{\beta}{k^2\lambda_{De}^2\nu_r}. \quad (22)$$

For a static test charge (viz., $V_t = 0$), the Landau damping term vanishes, and as a result, the DH potential is obtained in a similar form as that in Eq. (20) but with a new effective Debye length [48] $\lambda_{Def} = \lambda_{Dd}[1+\lambda_{Dd}^2(1+\frac{\beta}{\nu_r})/\lambda_{De}^2]^{-1/2}$ for an electron-dust plasma. Montgomery *et al.* [47] pointed out that one cannot rigorously neglect the Landau damping term when the speed of the test charge is much smaller than the thermal speed of the slower species in a dusty plasma. Thus, by writing Eq. (22) in a reciprocal form, we obtain

$$D^{-1} = \frac{k^2\lambda_{Def}^2}{k^2\lambda_{Def}^2+1}-\mathrm{i}\sqrt{\frac{\pi}{2}}\frac{\mu V_t}{V_{td}}\frac{k^2\lambda_{Def}^4}{\lambda_{Dd}^2}\left(k^2\lambda_{Def}^2+1\right)^{-2}. \quad (23)$$

The effective shielding length can be expressed as $\lambda_{Def} = \lambda_{Dd}\left[1+\left(1+\frac{\beta}{\nu_r}\right)/Z_{d0}\right]^{-1/2}$ in the limits $T_e = T_d$ and $n_{e0} \approx Z_{d0}n_{d0}$. Here, μ represents the angle between the wave vector k and the velocity V_t. By combining Eqs. (23) and (14), we can solve for the shielded potential in spherical polar coordinates to obtain $\phi_1(\boldsymbol{r},t) = \phi_{DH}(\boldsymbol{r},t)+\phi_{FF}(\boldsymbol{r},t)$. Here, $\phi_{DH}[=(Q_t/r)\exp(-r/\lambda_{Def})]$ corresponds to the short-range DH potential [49] with an effective Debye length λ_{Def}. On the other hand, the FF potential can be simplified by integrating over ϕ_k and μ as

$$\phi_{FF} = -\frac{2Q_t}{\sqrt{2\pi}}\frac{\xi}{r}\frac{V_t}{V_{td}}\frac{\lambda_{Def}^4}{\lambda_{Dd}^2}\frac{\partial}{\partial r}\int_0^\infty\frac{1}{r}\frac{\sin(kr)}{(k^2\lambda_{Def}^2+1)^2}\mathrm{d}k. \quad (24)$$

Now, by integrating Eq. (24) with respect to k, we finally arrive at the result

$$\phi_{FF} = \frac{4Q_t}{\sqrt{2\pi}r}\frac{\xi}{\lambda_{Dd}}\frac{V_t\lambda_{Def}}{V_{td}\lambda_{Dd}}\frac{\lambda_{Def}^3}{r^3}. \quad (25)$$

The expression in Eq. (25) represents the long-range FF potential of a slowly moving test charge and is only valid in the long-range limit, i.e., $r \gg \lambda_{Def}$. It is also important to note that this shielded potential decreases with the inverse cube of both the axial and radial distances from the test charge in a positive dust-electron plasma.

5 Results and discussion

As a first step, we normalize the expressions in Eqs. (17), (20), (21), and (25) for computational purposes by using the normalized variables $\bar{\omega} = \omega/\omega_{pd}$, $\bar{k} = k\lambda_{De}$, $\bar{\phi}_{DH} = \phi_{DH}/(Q_t/\lambda_{De})$, $\bar{\phi}_{WF} = \phi_{WF}/(Q_t/\lambda_{De})$, $\bar{\phi}_{FF} = \phi_{FF}/(Q_t/\lambda_{De})$, $\bar{\rho} = \rho/\lambda_{De}$, $\bar{\xi} = \xi/\lambda_{De}$, and $\bar{V}_t = V_t/C_{da}$. We also consider some numerical values that correspond to a laboratory plasma [49], for example, $n_{e0} \sim 10^9$ cm^{-3}, $n_{d0} \sim 10^7$ cm^{-3}, $Z_{d0} = 100$, $R = (0.1-0.05)$ μm, $J = 2\times10^{18}$ photons cm^{-2}·s^{-1}, $Y = 0.1$, and $W_e = 2.5$ eV. Furthermore, the values for the average thermal energies, $T_e = T_{ph} \sim 1$ eV and $T_e = T_d \sim 0.15$ eV, are respectively used to investigate the effects of the photoelectron and thermionic emission currents on the shielded potential. Relying on the above numerical values, other physical quantities,

namely, the electron plasma frequency $\omega_{pe} \sim 1.78 \times 10^9$ s^{-1}, the dust plasma frequency $\omega_{pd} \sim 9.3 \times 10^3$ s^{-1}, the electron and dust thermal speeds $V_{te} \sim 4.1 \times 10^7$ cm/s and $V_{td} \sim 21.88$ cm/s, the DA speed and electron Debye length $C_{da} = \omega_{pd}\lambda_{De} \equiv 218.85$ cm/s and $\lambda_{De} \sim 0.023$ cm, are computed. In addition, the electron absorption and dust-charge relaxation rates lead to the values $\nu_a \sim 7.3 \times 10^5$ s^{-1} and $\nu_r \sim 5.1 \times 10^5$ s^{-1} for the nonzero photoelectron emission and electron collection currents with $I_{th1} = 0$ for simplicity. However, even for a vanishing photoelectron emission current, the magnitude of ν_r (ν_a) is reduced to the value $\nu_r \sim 3 \times 10^5$ s^{-1}(remains constant). Similarly, we have also imposed the condition $\nu_r > \omega$ in this model to obtain the dielectric constant in Eq. (13) involving the DA waves.

Figure 1(a) shows the effects of a fluctuating dust-charge state (Z_{d1}) as well as the constant dust-charge state (Z_{d0}) on the normalized dispersion relation of the DA waves. The latter is significantly modified by the electron collection and photoemission currents through the charging equation $\partial_t Z_{d1} e = I_{e1} + I_{ph1}$. Here, the solid black curve highlights the impact of the nonzero dust-charge state $Z_{d1} \neq 0$, whereas the dashed blue curve corresponds to $Z_{d1} = 0$, which means that the dust grains are assumed to have a constant charge. The frequency of the DA wave varies in magnitude as a function of the wave number, and the modifications are found to be more prominent owing to the photoemission process rather than the contribution caused by the thermionic emission process through the equation $\partial_t Z_{d1} e = I_{e1} + I_{th1}$, as displayed in Fig. 1(b). Physically, the emission of electrons from the dust grains may be carried out by either photoelectron emission or thermionic emission, which could lead to an enhancement in the electron number density (in contrast to a negatively charged dusty plasma, which is not our focus in the present model) in the plasma system. Thus, the large electron concentration decreases the electron Debye length and results in an increase in the phase speed of the DA waves. However, the dust-charge perturbation effects through the factor $(1 + \beta/\nu_r)$ further decrease the electron Debye length as well as the phase speed (see the solid black curve in Fig. 1).

In the photoemission process, electrons are emitted by ultraviolet radiation and depend upon the dust material, dust polarity (the sign of the dust charge), and the source of irradiation; however, thermally emitted electrons exhibit a strong dependence on the dust surface temperature and its polarity. In fact, these electrons are sufficiently energetic that they can escape from the dust surface while overcoming the potential barrier between the dust surface and the ambient plasma. Hence, the average thermal energy associated with ultraviolet photoelectron and thermionic emission not only affects the spectrum of the DA waves but also modifies the test-charge DH and WF potentials $(\bar{\phi}_{DH}, \bar{\phi}_W)$ as a function of the axial distance $(\bar{\xi})$. The variations in the average thermal energy for $T_e = T_{ph}(\sim 1, 1.5, 2)$ eV and $T_e = T_d(\sim 0.13, 0.14, 0.145)$ eV are shown in Figs. 2 and 3, respectively, for fixed normalized test-charge speeds $V_t\,(= 0.9, 1)\, C_{da}$ with a grain radius $R = 0.1$ μm and a radial distance $\rho = 0.2\lambda_{De}$. The numerical values, e.g., $T_e = T_{ph} \sim 1$ eV [$(\sim 1, 1.5, 2)$ eV] and $T_e = T_d \sim 0.13$ eV [$(\sim 0.14, 0.145)$ eV] are typically found in the literature [50] for studying positive dust-electron plasmas [taken as nominal]. In both cases, the behavior of the DH potential [see Fig. 2(a) and Fig. 3(a)] exponentially decays as the thermal energy increases. However, the impact of the thermal energy is more obvious in case of photoelectron emission rather than thermionic emission. Figures 2(b) and 3(b) show the formation of an oscillatory WF behind the test charge when the DA speed approaches the test-charge speed (viz., $V_t \sim C_{da}$). Consequently, the amplitudes of the positive and negative potential regions decrease (increase) as the dust-charge relaxation rate decreases owing to the photoelectron emission current (thermionic emission current). The damping of oscillatory WF potential behind the test charge occurs for several Debye lengths in a positively charged dusty plasma. It is well-known [51] that the WF potential can be attractive for the positive-sign charges with the same

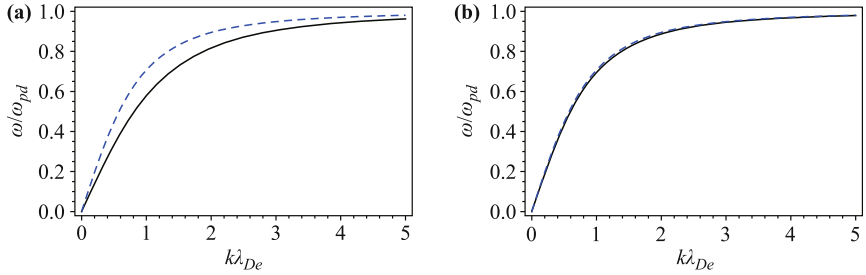

Fig. 1 The normalized wave frequency (ω/ω_{pd}) is plotted against the normalized wave number ($k\lambda_{De}$) for showing the effects of **(a)** photoelectron emission current and **(b)** thermionic emission current. The solid black curves represent the dust charging effects ($Z_{d1} \neq 0$), while the dashed blue curves show the absence of dust charging effects ($Z_{d1} = 0$). Other parameters are the same as given in Section 5.

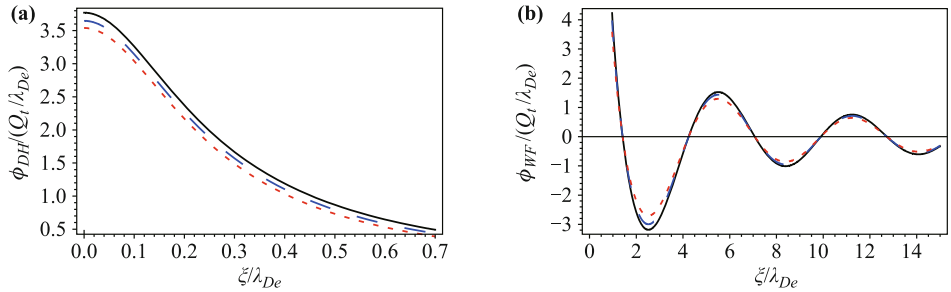

Fig. 2 The normalized DH potential $[\phi_{DH}/(Q_t/\lambda_{De})]$ and WF potential $[\phi_{WF}/(Q_t/\lambda_{De})]$ are plotted against the normalized axial distance (ξ/λ_{De}) in **(a)** and **(b)**, respectively, for varying the average thermal energy $T_e = T_{ph} = 1$ eV (*solid black curve*), 1.5 eV (*dashed blue curve*) and 2 eV (*red dotted curve*) with constant values of $V_t = 0.9C_{da}$ and $\rho = 0.2\lambda_{De}$. Other parameters are the same as given in Section 5.

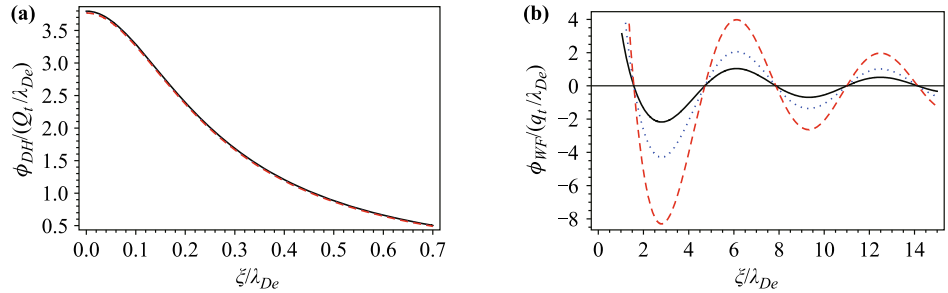

Fig. 3 The normalized DH potential $[\phi_{DH}/(Q_t/\lambda_{De})]$ and WF potential $[\phi_{WF}/(Q_t/\lambda_{De})]$ are plotted against the normalized axial distance (ξ/λ_{De}) in **(a)** and **(b)**, respectively, for taking $T_e = T_d = 0.13$ eV (*solid black curve*), 0.13 eV (*dashed blue curve*) and 0.145 eV (*red dotted curve*) with $V_t \sim C_{da}$ and $\rho = 0.2\lambda_{De}$. Other parameters are the same as given in Section 5.

Table 1 Typical parameters used in electron-dust laboratory plasmas.

(i) Normalized FF potential (ϕ_{FF}) caused by electron collection and photoemission currents with fixed $\rho = 0.02\lambda_{De}$ and $\xi = 0.8\lambda_{De}$.						
Z_{d0}	$T_e = T_{ph}$	ν_a/ν_r	$(\lambda_{Dd}/\lambda_{De})^2$	Λ	$g \approx [1 + \Lambda\nu_a(\lambda_{Dd}/\lambda_{De})^2/\nu_r]^2$	ϕ_{FF}
100	1 eV	1.42846	0.01	0.694473	1.01994	0.000152638
(ii) Normalized FF potential (ϕ_{FF}) caused by electron collection and thermionic emission currents with fixed $\rho = 0.02\lambda_{De}$ and $\xi = 0.8\lambda_{De}$.						
Z_{d0}	$T_e = T_d$	ν_a/ν_r	$(\lambda_{Dd}/\lambda_{De})^2$	Λ	$g \approx [1 + \Lambda\nu_a(\lambda_{Dd}/\lambda_{De})^2/\nu_r]^2$	ϕ_{FF}
100	0.15 eV	0.747528	0.01	0.104171	1.00156	0.00015544

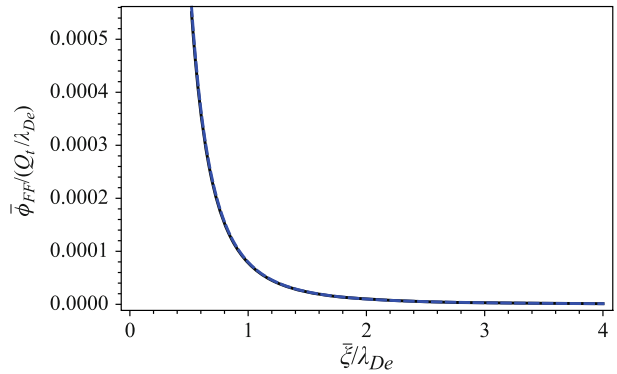

Fig. 4 The normalized FF potential $\bar{\phi}_{FF}$ [given by Eq. (25)] is plotted as a function of normalized axial distance $\bar{\xi}$ for photoelectron emission (*solid black curve*) and thermionic emission (*dashed blue curve*). Other parameters are the same as given in Section 5.

polarity under the conditions $\bar{V}_t\,(1 + \beta/\nu_r) > 1$ and $\cos\left(\bar{\xi}/\bar{V}_t\right) < 0$.

On the other hand, the normalized FF potential $\left(\bar{\phi}_{FF}\right)$ distribution [given by Eq. (25)] around a slow test charge is plotted as a function of the normalized axial distance $\bar{\xi}$ (see Fig. 4) for photoelectron and thermionic emission with a fixed dust-charge state $Z_{d0}\,(= 100)$ and test-charge speed $V_t\,(= 0.005C_{da})$. The solid black and dashed blue curves correspond to ultraviolet photoelectron and thermionic emission, respectively. It may be noted that the potential profiles overlap and exhibit similar behavior for different charging mechanisms. Since the normalized FF potential is inversely proportional to the parameters $\frac{1}{Z_{d0}}$, $\frac{1}{\left(\bar{\xi}^2+\bar{\rho}^2\right)^2}$, and $\frac{1}{(1+\beta/\nu_r Z_{d0})^2}$, any domi-

nant influence of dust-charge fluctuations does not appear in the profiles of the FF potential. This can also be confirmed from the table by comparing the normalized values of the FF potential caused by the ultraviolet photoelectron and thermionic emission currents. Note that the variation in the potential appears five digits beyond the decimal point; thus, it apparently does not modify the potential profiles. Hence, the dust-charge fluctuations have a negligibly small impact on the FF potential in an electron-dust plasma for specific laboratory parameters.

To summarize, we have considered a two-component dusty plasma containing electrons and positively charged fluctuating dust particulates. The inertialess electrons are assumed to follow the Boltzmann distribution, whereas the dust grains are taken as inertial and positively charged particles described by the Vlasov equation. In this model, the dust charging equation is employed to incorporate the effects of the electron collection, ultraviolet photoelectron emission, and thermionic emission currents. The dust-charge dynamics and the application of the space–time Fourier transform technique to the Vlasov–Poisson equations lead to a modified dielectric response function for DA waves and an expression for the test-charge potential in the limit of a large dust-charge relaxation rate. Numerical analyses are performed for DH, WF, and FF potentials to show the significant modifications due to the variation in the plasma parameters. Thus, the present results could be important in the context of dust crystallization/coagulation in positive dust-electron plasmas.

Acknowledgements S. Ali acknowledges the support from the Abdus Salam International Centre for Theoretical Physics (AS-ICTP) for his visit through the regular associateship scheme and Dr. M. H. Nasim for useful discussions.

References

1. T. Peter, Linearized potential of an ion moving through plasma, *J. Plasma Phys.* 44(02), 269 (1990)
2. T. Peter and J. Meyer-ter-Vehn, Energy loss of heavy ions in dense plasma (I): Linear and nonlinear Vlasov theory for the stopping power, *Phys. Rev. A* 43(4), 1998 (1991)
3. J. Neufeld and R. H. Ritchie, Passage of charged particles through plasma, *Phys. Rev.* 98(6), 1632 (1955)
4. J. R. Sanmartin and S. H. Lam, Far-Wake structure in Rarefield plasma flows past charged bodies, *Phys. Fluids* 14(1), 62 (1971)
5. L. Chen, A. B. Langdon, and M. A. Lieberman, Shielding of moving test particles in warm, isotropic plasma, *J. Plasma Phys.* 9(03), 311 (1973)
6. M. Nambu, S. V. Vladimirov, and P. K. Shukla, Attractive forces between charged particulates in plasmas, *Phys. Lett. A* 203(1), 40 (1995)
7. S. V. Vladimirov and M. Nambu, Attraction of charged particulates in plasmas with finite flows, *Phys. Rev. E* 52(3), R2172 (1995)
8. M. Salimullah and M. Nambu, Crystallization in a magnetized and inhomogeneous dusty plasma with streaming ions, *J. Phys. Soc. Jpn.* 69(6), 1688 (2000)
9. M. Nambu, B. J. Saikia, and T. Hada, Wake potential around a test dust particulate in a magnetized plasma with streaming ions, *J. Phys. Soc. Jpn.* 70(5), 1175 (2001)
10. M. Nambu, three-dimensional wake potential due to ion cyclotron waves in a flowing magnetized plasma, *Phys. Scr.* T98, 130 (2002)
11. M. H. Nasim, Energy loss of charged projectiles in a dusty plasma, Ph.D. thesis, Quaid-i-Azam University, Islamabad, Pakistan, 1999
12. H. Ikezi, Coulomb solid of small particles in plasmas, *Phys. Fluids* 29(6), 1764 (1986)
13. J. H. Chu and I. Lin, Direct observation of Coulomb crystals and liquids in strongly coupled RF dusty plasmas, *Phys. Lett. A* 72(25), 4009 (1994)
14. J. H. Chu, J. B. Du, and I. Lin, Coulomb solids and low-frequency fluctuations in RF dusty plasmas, *J. Phys. D* 27(2), 296 (1994)
15. H. Thomas, G. E. Morfill, V. Demmel, J. Goree, B. Feuerbacher, and D. Möhlmann, Plasma crystal: Coulomb crystallization in a dusty plasma, *Phys. Rev. Lett.* 73(5), 652 (1994)
16. Y. Hayashi and K. Tachibana, Observation of coulomb-crystal formation from carbon particles grown in a Methane plasma, *Jpn. J. Appl. Phys.* 33, L804 (1994)
17. A. Melzer, T. Trottenberg, and A. Piel, Experimental determination of the charge on dust particles forming Coulomb lattices, *Phys. Lett. A* 191(3–4), 301 (1994)
18. M. Nambu and H. Akama, Attractive potential between resonant electrons, *Phys. Fluids* 28(7), 2300 (1985)
19. N. N. Rao and P. K. Shukla, Nonlinear dust-acoustic waves with dust charge fluctuations, *Planet. Space Sci.* 42(3), 221 (1994)
20. J. X. Ma and P. K. Shukla, Compact dispersion relation for parametric instabilities of electromagnetic waves in dusty plasmas, *Phys. Plasmas* 1(5), 1506 (1995)
21. R. K. Varma, P. K. Shukla, and V. Krishan, Electrostatic oscillations in the presence of grain-charge perturbations in dusty plasmas, *Phys. Rev. E* 47(5), 3612 (1993)
22. P. K. Shukla, in: The Physics of Dusty Plasmas, edited by P. K. Shukla, D. A. Mendis, and V. W. Chow, Singapore: World Scientific, 1996
23. F. Melandsc, T. Aslaksen, and O. Havnes, A new damping effect for the dust-acoustic wave, *Planet. Space Sci.* 41(4), 321 (1993)

24. M. H. Nasim, P. K. Shukla, and G. Murtaza, Effect of dust charge fluctuations on energy loss of a test dust charged particulate in a dusty plasma, *Phys. Plasmas* 6(5), 1409 (1999)
25. M. H. Nasim, A. M. Mirza, G. Murtaza, and P. K. Shukla, Energy loss of a test charge in dusty plasmas: collective and individual particle contributions, *Phys. Scr.* 59(5), 379 (1999)
26. S. Ali, M. H. Nasim, and G. Murtaza, Effects of dust-charge fluctuations on the potential of an array of projectiles in a partially ionized dusty plasma, *Phys. Plasmas* 10(11), 4207 (2003)
27. M. Horanyi, G. E. Morfill, and E. Griin, Mechanism for the acceleration and ejection of dust grains from Jupiter's magnetosphere, *Nature* 363(6425), 144 (1993)
28. O. Havnes, J. Trøim, T. Blix, W. Mortensen, L. I. Næsheim, E. Thrane, and T. Tønnesen, First detection of charged dust particles in the Earth's mesosphere, *J. Geophys. Res.* 101(A5), 10839 (1996)
29. V. E. Fortov, A. P. Nefedov, O. F. Petrov, A. A. Samarian, and A. V. Chernyschev, Particle ordered structures in a strongly coupled classical thermal plasma, *Phys. Rev. E* 54(3), R2236 (1996)
30. A. A. Samarian, O. S. Vaulina, A. P. Nefedov, V. E. Fortov, B. W. James, and O. F. Petrov, Positively charged particles in dusty plasmas, *Phys. Rev. E* 64, 056407 (2001)
31. M. Rosenberg and D. A. Mendis, UV-induced Coulomb crystallization in a dusty gas, *IEEE Trans. Plasma Sci.* 23(2), 177 (1995)
32. P. K. Shukla and D. Resendes, Dust acoustic waves with dust charge fluctuations — revisited, *Phys. Plasmas* 7(5), 1614 (2000)
33. P. K. Shukla, Dust acoustic wave in a thermal dusty plasma, *Phys. Rev. E* 61, 7249 (2000)
34. S. Ghosh, Dust acoustic shock waves in two-component dusty plasma, *New J. Phys.* 5, 142 (2003)
35. M. Horanyi, B. Walch, S. Robertson, and D. Alexander, Electrostatic charging properties of Apollo 17 lunar dust, *J. Geophys. Res.* 103(E4), 8575 (1998)
36. C. K. Goertz, Dusty plasmas in the solar system, *Rev. Geophys.* 27(2), 271 (1989)
37. G. L. Delzanno, G. Lapenta, and M. Rosenberg, Attractive potential around a thermionically emitting microparticle, *Phys. Rev. Lett.* 92(3), 350021 (2004)
38. S. K. Paul, *IJCIT* 2, 25 (2012)
39. P. K. Shukla and A. A. Mamun, Introduction to Dusty Plasma Physics, Bristol, U.K.: Institute of Physics Publishing Ltd., 2002
40. M. Sodha and S. Guha, Physics of Colloidal Plasmas, *Adv. Plasma Phys.* 4, 219 (1971)
41. M. Rosenberg, D. A. Mendis, and D. Sheenan, UV-induced Coulomb crystallization of dust grains in high-pressure gas, *IEEE Trans. Plasma Sci.* 24(6), 1422 (1996)
42. S. A. Khrapak, A. P. Nefedov, O. F. Petrov, and O. S. Vaulina, Dynamical properties of random charge fluctuations in a dusty plasma with different charging mechanisms, *Phys. Rev. E* 59, 6017 (1999)
43. D. B. Fried and S. D. Conte, The Plasma Dispersion Function, New York: Academic Press, 1961
44. N. A. Krall and A. W. Trivelpiece, Principles of Plasma Physics, New York: McGraw-Hill, 1973
45. X. G. Wang and Q. B. Luan, Low frequency Whistler waves excited in fast magnetic reconnection processes, *Front. Phys.* 8(5), 585 (2013)
46. Z. H. Hu, M. D. Chen, and Y. N. Wang, Current neutralization and plasma polarization for intense ion beams propagating through magnetized background plasmas in a two-dimensional slab approximation, *Front. Phys.* 9(2), 226 (2014)
47. D. Montgomery, G. Joyce, and R. Sugihara, Inverse third power law for the shielding of test particles, *Plasma Phys.* 10(7), 681 (1968)
48. S. A. Khrapak and G. Morfill, Waves in two component electron-dust plasma, *Phys. Plasmas* 8(6), 2629 (2001)
49. P. Debye and E. Hückel, The theory of electrolytes (I): Lowering of freezing point and related phenomena, *Phys. Z.* 24, 185 (1923)
50. M. Rosenberg and P. K. Shukla, On beam-plasma interaction in a dust-electron plasma, *IEEE Trans. Plasma Sci.* 29(2), 202 (2001)
51. P. K. Shukla and N. N. Rao, Coulomb crystallization in colloidal plasmas with streaming ions and dust grains, *Phys. Plasmas* 3(5), 1770 (1996)